iScience

CellPress

Article

Tolerance of Perovskite Solar Cell to High-Energy Particle Irradiations in Space Environment

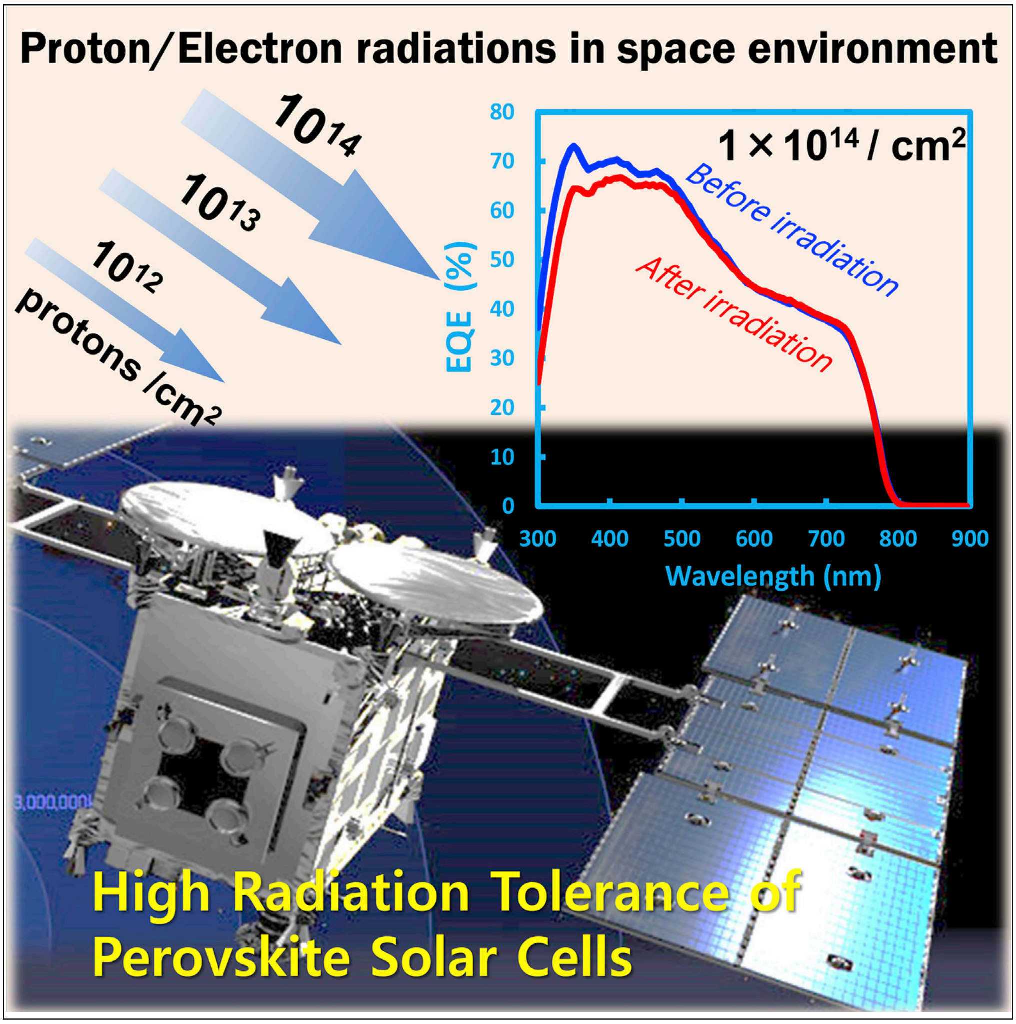

Yu Miyazawa, Masashi Ikegami, Hsin-Wei Chen, Takeshi Ohshima, Mitsuru Imaizumi, Kazuyuki Hirose, Tsutomu Miyasaka

miyasaka@toin.ac.jp

HIGHLIGHTS

Lead halide perovskites have extreme stability against electron and proton irradiations

Radiation tolerance of perovskite solar cells can exceed those of Si- and GaAs-based cells

Proton beam focused to perovskite absorber revealed high stability up to 10^{14} protons/cm^2

Our study shows the usefulness of lightweight perovskite solar cells in satellite missions

Miyazawa et al., iScience *2*, 148–155
April 27, 2018 © 2018 The Author(s).
https://doi.org/10.1016/j.isci.2018.03.020

iScience

CellPress

Article

Tolerance of Perovskite Solar Cell to High-Energy Particle Irradiations in Space Environment

Yu Miyazawa,[1] Masashi Ikegami,[2] Hsin-Wei Chen,[3] Takeshi Ohshima,[4] Mitsuru Imaizumi,[1] Kazuyuki Hirose,[1] and Tsutomu Miyasaka[2,5,*]

SUMMARY

Materials to be used in the space environment have to withstand extreme conditions, particularly with respect to cosmic particle irradiation. We report robust stability and high tolerance of organolead trihalide perovskite solar cells against high-fluence electron and proton beams. We found that methylammonium and formamidinium-based lead iodide perovskite solar cells composed of TiO_2 and a conductive polymer, as electron and hole transport materials, can survive against accumulated dose levels up to 10^{16} and 10^{15}particles/cm^2 of electrons (1 MeV) and protons (50 KeV), respectively, which are known to completely destroy crystalline Si-, GaAS-, and InGaP/GaAs-based solar cells in spacecraft. These results justify the superior tolerance of perovskite photovoltaic materials to severe space radiations and their usefulness in satellite missions.

INTRODUCTION

Organic-inorganic metal halide perovskite (Mitzi, 1999) as solution-processable photovoltaic material (Kojima et al., 2009) has established as an excellent photovoltaic material due to its advantages of being a thin film absorber (<0.5 μm) and having a cost-efficient high photovoltaic performance (Miyasaka, 2015; Park et al., 2016). High extinction coefficient (10^5 cm^{-1}) of visible light absorption and defect-tolerant properties of the perovskites have enabled the use of thin film as absorber and generation of high voltage in photovoltaic performance, which has led to power conversion efficiency of solar cell beyond 22% (Yang et al., 2017; Green and Ho-Baillie, 2017). The device stability has also been improved by preparation of uniform perovskite layers of large grains that minimize grain boundaries and defects (Brenner et al., 2016; Saliba et al., 2016a). In particular, multi-cation perovskites having methylammmonium (MA), formamidinium (FA), and Cs as cations with I and Br as halide tend to exhibit stable high efficiency and robust stability against light and heat (Saliba et al., 2016a, 2016b; Singh and Miyasaka, 2017). Taking advantage of the light weight and mechanical flexibility (Kogo et al., 2016; Giacomo et al., 2016), perovskite solar cell will see its usefulness as a power source mounted on transportation objects like electric vehicles, and more promisingly on spacecraft and satellites. In space applications, however, severe environments that deteriorate most semiconductors of solar cells are high-energy cosmic particles such as electron and proton (Anspaugh, 1989, 1996; Morita et al., 1997). Our study focused on the potential stability of the perovskite solar cell being exposed to the space environment. Spacecrafts circulating on low earth orbit of outer space are exposed to irradiations of energetic particles, typically electrons (incident rate of 1-MeV electron, ~6×10^3 cm^{-2}s^{-1}) and protons (incident rate of 100-KeV proton, ~1×10^4 cm^{-2}s^{-1}). Here, PB causes significant damage to degrade semiconductor materials of solar cells with a particle fluence that is two orders of magnitude lower than that of electron irradiation. For example, triple junction solar cells such as InGaP/InGaAs/Ge degrade by PBs of low-energy range (30–250 KeV) with a fluence level of 10^{12} particle cm^{-2} (Sumita et al., 2003; Imaizumi et al., 2017), whereas protons of energy >10 MeV can penetrate thin semiconductor layers and hence cause much less damage (Sumita et al., 2003). There have been two reports to date on the proton-irradiated lead halide perovskite solar cell (Lang et al., 2016; Brus et al., 2017). Brus et al. (2017) showed significantly high proton tolerance of MA perovskite cells compared with crystalline Si solar cells. Using high-energy 68-MeV proton specifically, both studies found that the perovskite can be durable under proton fluence up to 10^{13} cm^{-2}. However, as we demonstrate in this report, such high proton energy can penetrate the perovskite absorber layer without causing significant collision event, making correct assessment of proton tolerance difficult.

Stability requirements of satellite solar cells are not limited to particle radiations but are also directed to thermal stability. Solar cells in satellite missions are exposed to cyclic temperature changes

[1]Japan Aerospace Exploration Agency (JAXA), 3-1-1 Yoshinodai, Chu-o-ku, Sagamihara, Kanagawa 252-5210, Japan

[2]Graduate School of Engineering, Toin University of Yokohama, Kuroganecho 1614, Aoba, Yokohama, Kanagawa 225-8503, Japan

[3]Graduate School of Arts and Sciences, The University of Tokyo, Komaba 3-8-1, Meguro-ku, Tokyo 153-8902, Japan

[4]National Institutes for Quantum and Radiological Science and Technology, Watanuki 1233, Takasaki, Gunma 370-1292, Japan

[5]Lead Contact

*Correspondence: miyasaka@toin.ac.jp

https://doi.org/10.1016/j.isci.2018.03.020

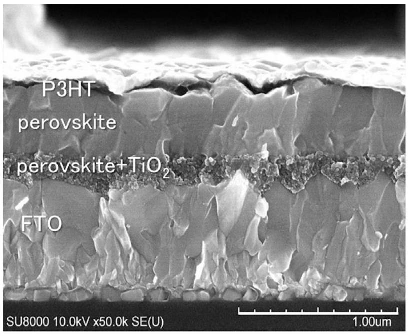

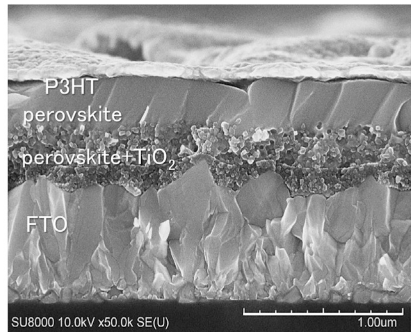

Figure 1. Cross-Sectional SEM Views of the P3HT-based FAMAPb(IBr)$_3$ (left) and $MAPbI_3$ (right) Perovskite Solar Cells Employed for Radiation Tolerance Measurements

Scale bar represents 1 μm. For photovoltaic performance of these cells, see Supplemental Information, Figure S1.

(±80–100°C) in earth orbit. Perovskite solar cells exhibit relatively low thermal stability (<150°C) affected by the kinds of organic materials in addition to the intrinsic property of perovskite unlike inorganic semiconductor solar cells (Si, GaAs, CdTe, etc.), which are thermally highly stable. As for the choice of absorber, FA-mixed perovskites are thermally stable up to 150°C, whereas pure MA exhibits instability due to evaporation of MA at high temperature (>120°C) and under vacuum (Smecca et al., 2016). In combination with the absorber, carrier transport materials play a key role in improving stability. Metal oxides such as TiO_2 and SnO_2 widely employed as electron transport materials (ETMs) are thermally stable. However, hole transport materials (HTMs) are generally organic materials when they must cap the perovskite layer by low-temperature solution process. As the most popular small molecule HTM, LiTFSI-doped spiro-OMeTAD [2,2,7,7-tetrakis(N,N-di-p-methoxyphenylamine)-9,9-spirobifluorene] is known to trigger degradation of perovskite solar cells at high temperatures (>80°C) accompanied by morphological changes (Jena et al., 2017), physical degradation (Li et al., 2016), and chemical oxidation (Sanchez and Mas-Marza, 2016). As heat-resistant alternatives, polymer HTMs such as phenylenevinylene (PPV) derivatives and poly(3-hexylthiophene-2,5-diyl) (P3HT) are stable at temperatures up to 110°C and show durable performance of perovskite cells with a moderate efficiency of 6%–8% (Chen et al., 2016). In our space tolerance study, we chose perovskite device structures using TiO_2 as ETM and P3HT as HTM, both of which exhibited sufficient thermal stability against temperature changes between −80°C and 100°C. Using these TiO_2 ETM-based perovskite devices, we discovered that the perovskite absorbers could have remarkably high stability and tolerance to large dose of electron and proton irradiations in space environment. In this report, we demonstrate that the perovskite solar cell could survive under exposure to proton radiation fluence up to 10^{15} particles cm^{-2}, an extremely high level of collision that destroys Si and GaAs semiconductors.

RESULTS AND DISCUSSION

Device Fabrication

Lead halide perovskites of different cation/anion compositions were prepared by spin-coating lead halide and organic halide precursors on the double layer of TiO_2 compact layer (thickness, ~50 nm) and mesoporous layer (thickness, ~200 ± 50 nm) formed on transparent conducive glass or quartz substrate (Lee et al., 2012; Singh and Miyasaka, 2017). Our study focused on two typical perovskite compositions, which are mixed cation/halide perovskites $Cs_xFA_{0.85}MA_{0.15}Pb(I_{0.85}Br_{0.15})_3$ (x < 0.05) (Saliba et al., 2016a; Singh and Miyasaka, 2017), abbreviated as FAMAPb(IBr)$_3$, and Cl-doped $MAPbI_{3-x}Cl_x$ (Lee et al., 2012), where MA and FA are methylammonium and formamidinium cations, respectively. Indium tin oxide (ITO)-coated quartz substrate was specifically employed on EB irradiation, which can damage soda glass substrate. HTM layer was P3HT (molecular weight, 36,000–44,000), which was spin-coated on perovskite layer to form a thin 30- to 50-nm thick film. Au counterelectrode was thermally deposited on top of the HTM layer. The cell substrate size was 1.25 × 1.25 cm, on which 5 × 5-mm square-shaped solar cell was fabricated (detailed experimental procedures are given in Supplemental Information, Transparent Methods).

Figure 1 shows the cross-sectional SEM images of FAMAPb(IBr)$_3$ and $MAPbI_3$ solar cells. Thickness of the perovskite absorber, including the mesoporous TiO_2 layer filled with perovskite and P3HT that occupies

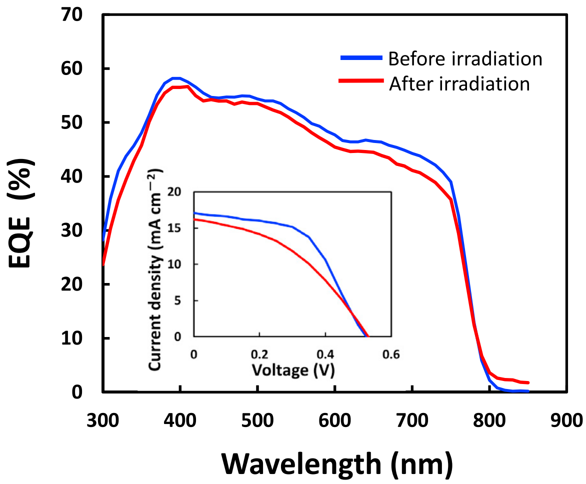

Figure 2. Photocurrent EQE Action Spectra and J-V Performance (insertion) of the P3HT-$MAPbI_3$ Perovskite Solar Cell Recorded before and after the 1 MeV EB Irradiation with a High Fluence of 1×10^{16} Particles cm^{-2}

EQE data are represented as mean $\pm$1%. See also J-V curves of other perovskite cells (before irradiation) in Figure S1. Because EB irradiation causes local temperature increase, EB tests were only conducted for P3HT-based cell structures that have passed thermal stability test as shown in Supplemental Information, Table S2, and Figure S2.

the gap between perovskite absorber and Au electrode, are around 500 nm and 30 nm, respectively. Photocurrent density-voltage (J-V) characteristics collected for 15 cells of each cell structure are given in Transparent Methods (Table S1) with J-V curves of typical devices (Figure S1). $FAMAPb(IBr)_3$/P3HT cells showed open circuit voltage (V_{OC}) of 0.94 V, much higher than the V_{OC} of $MAPbI_3$/P3HT cells (<0.7 V) while they gave a low fill factor (FF) compared with $MAPbI_3$/P3HT cells. As results, power conversion efficiency (PCE) was comparable between the two cells and the highest value of 8.2% was obtained for as-prepared $MAPbI_3$/P3HT cell with relatively small hysteresis. For the samples of electron and proton irradiation, we chose a group of the largest number of $FAMAPb(IBr)_3$/P3HT and $MAPbI_3$/P3HT cells for comparison. Before irradiation, all cells (not encapsulated) are stored in dark at room temperature for 5–7 days to get stabilized efficiency. The stabilized PCE was in the range of 4.6%–4.8%, which lasted for about 1 week during which irradiation tests were conducted. Although the PCE is low, we could not fabricate another type of more efficient and stable perovskite device that is durable under high impacts of temperature changes (−80°C to +100°C).

Thermal Stability Examinations

Before radiation experiments, the thermal stability of P3HT-based $FAMAPb(IBr)_3$ and $MAPbI_3$ perovskite cells was examined. Cells were encapsulated by sandwiching and gluing them with glass sheets and a hot-melt-type gasket sealing film and then packed in aluminum-covered evacuated container. Sample cells in the container were exposed to temperatures of +100°C and −80°C, corresponding to the temperatures of satellite orbit in hemispheres of globe with and without exposure to sunlight, respectively. As results, all P3HT-based encapsulated cells mostly maintained performance without losing J_{SC} and V_{OC} at +100°C and −80°C for up to 1000 min (16.7 hr) (Table S2). However, cells without encapsulation degraded losing >50% of J_{SC} and showing yellow deposits due to PbI_2. This indicates that encapsulation against evaporation of MA and FA at high temperature under vacuum is mandatory for satellite applications. As a reference, our stability test also included spiro-OMeTAD-based $MAPbI_3$ cells. Although the initial PCE was high (15%–17%), the encapsulated cell kept at 100°C resulted in 80% reduction in PCE within first 2 hr and all cells underwent drastic degradation or inoperability after 16.7 hr. Such deterioration is assumed to be due to thermal degradation of spiro-OMeTAD. In contrast, P3HT-based $FAMAPb(IBr)_3$ cells sustained cell performance at 100°C for prolonged time up to 120 hr (5 days) without significant loss in J_{SC} and V_{OC} (Table S2, Figure S2).

Electron Beam Tolerance of Perovskite Solar Cells

Electronbeam (EB) exists in space as a major cosmic ray in terms of number of particles. To investigate electron collision damage, EB irradiation to perovskite cells was conducted by means of a Cockcroft-Walton

Photovoltaic Parameters	Perovskite Solar Cell (P3HT-$MAPbI_3$)					Crystalline Si Solar Cell (Yamaguchi et al., 1996)	III/V (InGaP/InGaAs/Ge) Solar Cell (Cho et al., 2009)
	Cell 1	Cell 2	Cell 3	Average	Cell without Exposure		
J_{SC}	95%	100%	100%	98%	96%	80%	82%
V_{OC}	100%	97%	94%	97%	100%	80%	82%
FF	100%	103%	85%	96%	104%	93%	92%
P_{max}	95%	100%	80%	92%	100%	60%	62%

Table 1. Electron Beam (EB) Tolerance of P3HT Perovskite Solar Cells after Exposure to a Fluence of 1×10^{16} Particles cm^{-2} when Compared with Tolerance of Si and Triple-Junction III-IV Compound Semiconductor Solar Cells

Remaining factors (%) of photovoltaic parameters after EB exposure are listed.

accelerator. Encapsulated P3HT perovskite solar cells were exposed to 1 MeV EB irradiation at particle rate of 1×10^{12} particles cm^{-2} s^{-1} for 167 min (10^4 s), which creates an accumulated EB fluence of 1×10^{16} particles cm^{-2}. As results, EB-induced damage (change) on cell performance was found to be very small. J_{SC}, V_{OC}, and PCE for three cells maintained at 99% ± 4%, 97 ± 3%, and 93 ± 13%, respectively, of the initial values. Figure 2 shows the external quantum conversion efficiency (EQE) action spectra of photocurrent measured for P3HT-$MAPbI_3$ cell before and after the EB irradiation. Although J-V characteristics showed a drop in FF, no degradation was observed in EQE. Table 1 summarizes EB-induced changes in photovoltaic parameters of P3HT-$MAPbI_3$ perovskite cell compared with reported values for crystalline silicon (Yamaguchi et al., 1996) and triple-junction III-V compound solar cells (Cho et al., 2009). All perovskite cells demonstrated sufficiently high durability against high-fluence EB compared with Si and III-V compound solar cells. Generally, the EB tolerance of solar cells increases with use of a thinner light absorber, which has higher optical absorption coefficient. The combination of thin film and large carrier diffusion length of the perovskite semiconductor (>1 μm) (Stranks et al., 2013) is advantageous for raising radiation tolerance because photogenerated carriers in the presence of radiation-induced defects and traps still have sufficient diffusion to contribute to power generation.

Proton Irradiation Tolerance of Perovskite Solar Cells

Proton beam (PB) is composed of positively charged hydrogen nucleus with energy ranging from 100 KeV to hundreds of MeV per particle. Because of the greater mass of proton than electron (>2000 times), damage of materials by proton collision occurs at particle fluence generally two orders of magnitude smaller than that of electron. In our tolerance test, PB was irradiated from the Au counterelectrode side to avoid influence of thick glass substrate in PB penetration. This enables to concentrate the proton collision event at the depth of perovskite layer near Au electrode. In perovskite solar cell, stopping position of protons, which is a function of proton energy and density (mass) of material, was determined by the computer program SRIM/TRIM (Stopping and Range of Ions in Matter/Transport of Ions in Matter) using proton energies ranging from 50 KeV to 60 MeV. The result is displayed in Figure 3. A 50-KeV PB incident to the P3HT-$MAPbI_3$ cell gave a proton penetration depth mostly located at the depth of perovskite layer in the multilayered structure. Figure 3B shows how collision rate (number per proton particle) inside the cell is distributed between layered structures. The result corroborates that 50-KeV PB concentrates its collision event at the perovskite layer, whereas high-energy 60-MeV beam mostly penetrates the thin perovskite layer without substantial collision events. With other proton energies investigated, we decided that 50 KeV is best suited to stop proton particles at the perovskite layer. PB tolerance of perovskite ($MAPbI_3$) solar cells has been studied by Lang et al.(2016) and Brus et al.(2017) using a common Methyl [6,6]-phenyl-C61-butyrate (PCBM)-based organic type inverse structure cell. Despite high initial efficiency (11%–12%), both irradiated and non-irradiated (control) cells degraded to 4%–5% during irradiation tests (affected by light soaking), whereas our control cells maintained initial efficiency so that change of cell performance was focused on influence of EB or PB irradiation. In these studies, 68-MeV PB employed showed excellent tolerance of perovskite cell over Si cells to proton impacts up to 10^{13} particles cm^{-2}. However, based on our analysis, the 68 MeV energy was apparently too high to stop protons at the target perovskite layer. Our thermally durable perovskite cells were subjected to 50 KeV proton irradiation at an incident rate of 3×10^{11} $cm^{-2}s^{-1}$. This rate is 10^7 times larger than the natural value of space environment (low earth orbit) and a highly accelerated condition. Fluence was varied between

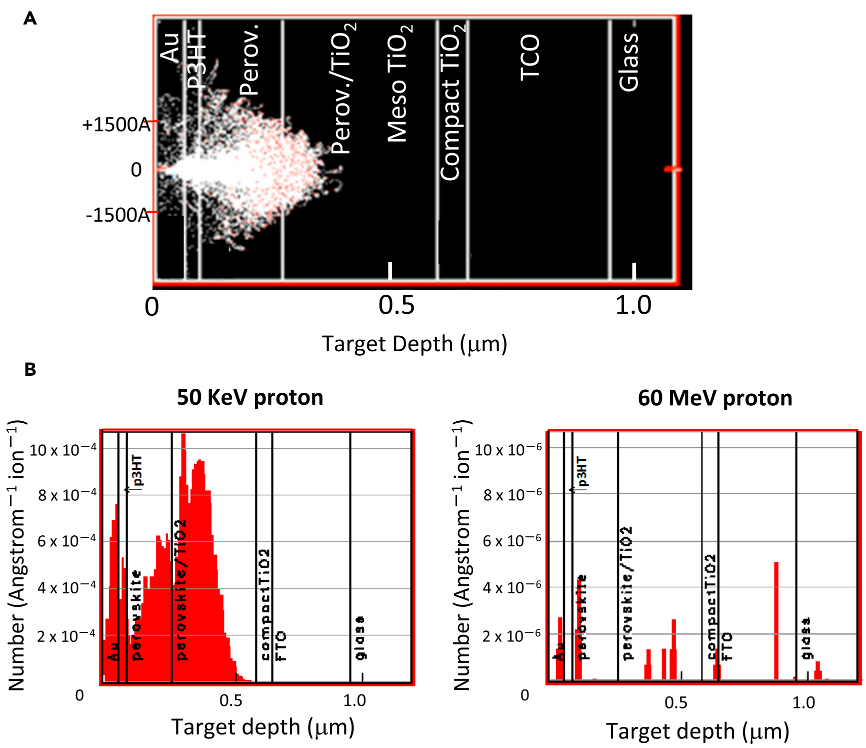

Figure 3. SRIM/TRIM Analysis of Proton-Induced Collision Event in Perovskite Solar Cell

(A) A profile of 50 KeV PB penetration depth along the depth of multilayered structure in the MA perovskite cell determined by SRIM/TRIM analysis.

(B) Experimentally detected number of vacancies and defects per angstrom ion when $MAPbI_3$ perovskite solar cells are irradiated by protons with energies of 50 KeV (left) and 60 MeV (right), respectively. Data were presented as mean value of 10,000 times irradiation of proton. See also the cell cross-sectional structure in Figure 1.

1×10^{12} and 1×10^{15} particles cm^{-2} (corresponding to 3.3–3300 s as duration time). Here, 1×10^{14} particles cm^{-2} is equivalent to a magnitude in low earth orbit for more than 10 years. The results of photovoltaic performance are summarized in Figures 4 and 5. We found that both of $MAPbI_3$ and $FAMAPb(IBr)_3$ cells have high stability and tolerance in the wide range of PB fluence employed. Figures 4A and 4B show changes of photocurrent EQE spectra before and after PB irradiation at fluences of 1×10^{13} and 1×10^{14} particles cm^{-2}, respectively. Higher fluence of 1×10^{14} tends to cause non-uniform changes in spectral response of photocurrent. However, PB-induced change was small and photovoltaic performance of $MAPbI_3$ and $FAMAPb(IBr)_3$ cells survived substantially. Figure 5 plots PB-induced changes in J_{SC}, V_{OC}, and PCE against 4 order range of fluences collected for groups of 4 or 5 sample cells. Here, $FAMAPb(IBr)_3$ cell showed a sign of degradation at 1×10^{14} particles cm^{-2} as reflected in EQE spectra (Figure 4B). However, no change was detected in the analysis of X-ray diffraction patterns and none of the cells exhibited color change indicative of PbI_2 produced by PB damage (Figure S3).

We further investigated the impact of high PB fluence up to 1×10^{15} particles cm^{-2} on $FAMAPb(IBr)_3$ using a group of 10 sample cells. Apparently, the cell was found to start degrading at this extreme dose level. However, to our surprise, some cells could still have photovoltaic activity with half reduction of PCE. As long as our tolerance test of space-aid solar cells is concerned, no solar cells (Si, CIGS, GaAs, etc.) could survive under proton fluence level of 1×10^{15} particles cm^{-2} (Anspaugh, 1989, 1996; Morita et al., 1997; Sumita et al., 2003; Imaizumi et al., 2017). Our experiments corroborate remarkably high tolerance of perovskite solar cells against space particle irradiation. We consider that the radiation tolerance of perovskite is endowed by the nature of considerably thin absorber film (<500 nm), large carrier diffusion length that exceeds absorber thickness, and defect tolerance of free carriers, all of which can minimize the influence of radiation-induced defects on photovoltaic performance. Our finding endorses usefulness of the perovskite cell for satellite mission.

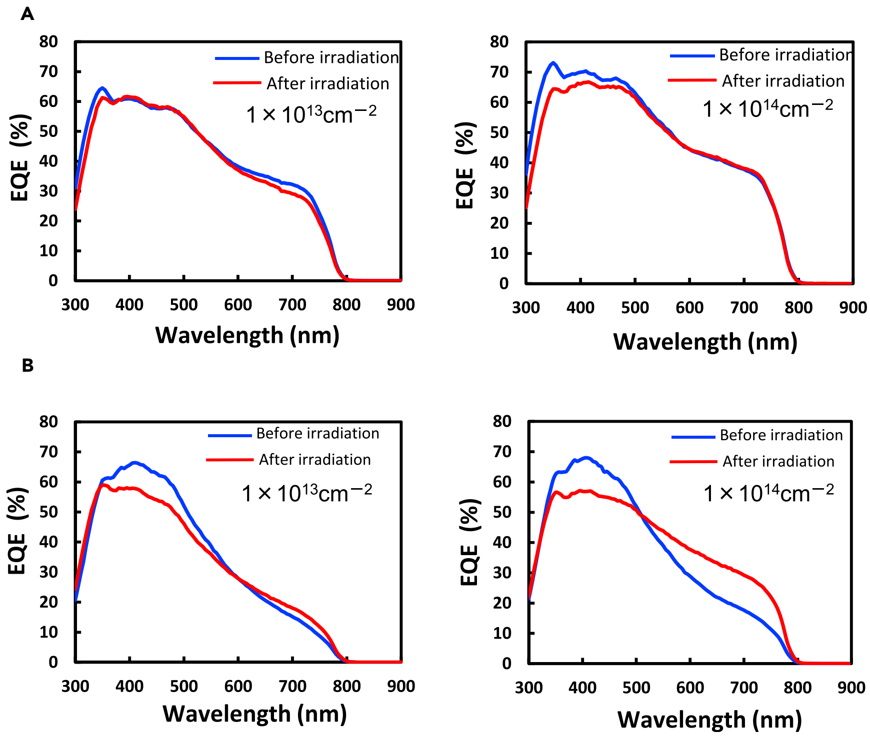

Figure 4. Influence of PB Irradiation on $MAPbI_3$ and $FAMAPb(IBr)_3$ Perovskite Solar Cells Detected by the Change in Photocurrent EQE Action Spectra before and after PB Irradiation

(A) Changes of EQE spectrum for $MAPbI_3$ perovskite cell before and after exposure to PB fluences of 1×10^{13} (left) and 1×10^{14} particles cm^{-2} (right).

(B) Changes of EQE spectrum for $FAMAPb(IBr)_3$ perovskite cell before and after exposure to PB fluences of 1×10^{13} (left) and 1×10^{14} particles cm^{-2} (right). See also Supplemental Information, Figure S3 for observation of color change before and after PB irradiation.

METHODS

All methods can be found in the accompanying Transparent Methods supplemental file.

SUPPLEMENTAL INFORMATION

Supplemental Information includes Transparent Methods, three figures, and two tables and can be found with this article online at https://doi.org/10.1016/j.isci.2018.03.020.

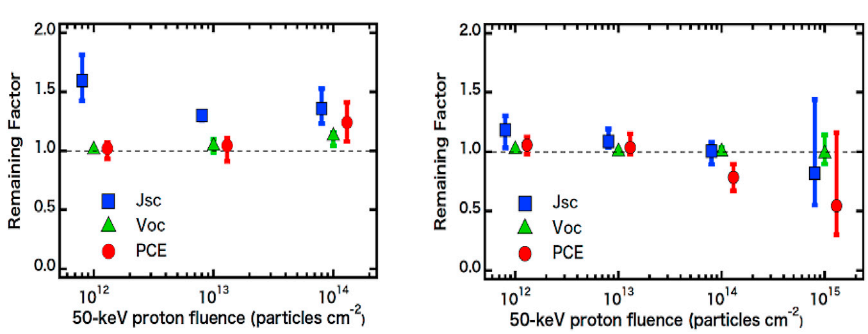

Figure 5. Changes of Photovoltaic Characteristics (J_{SC}, V_{OC}, P_{max}, and PCE) in $MAPbI_3$ (left) and $FAMAPb(IBr)_3$ (right) Perovskite Cells as a Function of PB Fluence

Values are normalized for unity at initial magnitudes. Data are represented as mean value of 4 cells with error bars as distribution of values.

ACKNOWLEDGMENTS

This research was supported by Japan Science and Technology Agency (JST), Advanced Low Carbon Technology (ALCA). T. M. and M. Ikegami thank Dr. Yoshitaka Sanehira for SEM measurements and Dr. Youhei Numata, Dr. Gyumin Kim, Mr. Ashish Kulkarni, Mr. Peerathat Pinpithak, and Mr. Tomoyuki Tobe for their assistance in perovskite device fabrication.

AUTHOR CONTRIBUTIONS

The experiments were conceived by Y.M., M. Imaizumi., K.H., and T.M. Material synthesis and device fabrication were conducted by H.-W.C. and M. Ikegami. Radiation tolerance measurements were performed by T.O., Y.M., M. Imaizumi., and K.H. Data were analyzed by Y.M., M. Imaizumi., M. Ikegami., and T.M. The results were interpreted by Y.M., M. Imaizumi., M. Ikegami, and T.M. SRIM/TRIM analysis was conducted by Y.M., K.H., and M. Imaizumi. The manuscript was written by Y.M. and T.M.

DECLARATION OF INTERESTS

The authors declare no competing interests.

Received: January 4, 2018
Revised: February 23, 2018
Accepted: March 1, 2018
Published: April 27, 2018

REFERENCES

Anspaugh, B.E. (1989). Solar Cell Radiation Handbook (JPL Publication).

Anspaugh, B.E. (1996). GaAs Solar Cell Radiation Handbook (JPL Publication).

Brenner, T.M., Egger, D.A., Kronik, L., Hodes, G., and Cahen, D. (2016). Hybrid organic–inorganic perovskites: low-cost semiconductors with intriguing charge-transport properties. Nat. Mater. *1*, 1–16.

Brus, V.V., Lang, F., Bundesmann, J., Seidel, S., Denker, A., Rech, B., Landi, G., Neitzert, H.C., Rappich, J., and Nickel, N.H. (2017). Defect dynamics in proton irradiated $CH_3NH_3PbI_3$ perovskite solar cells. Adv. Electron. Mater. *3*, 1600438.

Chen, H.-W., Huang, T.-Y., Chang, T.-H., Sanehira, Y., Kung, C.-W., Chu, C.-W., Ikegami, M., Miyasaka, T., and Ho, K.C. (2016). Efficiency enhancement of hybrid perovskite solar cells with MEH-PPV hole-transporting layers. Sci. Rep. *6*, 34319.

Cho, B., Davis, J., Hise, L., Korostyshevsky, A., Smith, G., Ley, A.V., Sharps, P., Varghese, T., and Stan, M. (2009). Qualification testing of the ZTJ GaInP2/GaInAs/Ge solar cell to the AIAA S-111 standard, 34th IEEE Photovoltaic Specialists Conference, Philadelphia, PA, USA, 07–12 June (SolAero Technologies Co. ZTJ Space Solar Cell data: http://solaerotech.com/wp-content/uploads/2015/03/ZTJ-Datasheet.pdf.)

Giacomo, F.D., Fakharuddin, A., Jose, R., and Brown, T.M. (2016). Progress, challenges and perspectives in flexible perovskite solar cells. Energy Environ. Sci. *9*, 3007–3035.

Green, M.A., and Ho-Baillie. (2017). Perovskite solar cells: the birth of a new era in photovoltaics. ACS Energy Lett. *2*, 822–830.

Imaizumi, M., Nakamura, T., Takamoto, T., Oshima, T., and Tajima, M. (2017). Radiation degradation characteristics of component subcells in inverted metamorphic triple-junction solar cells irradiated with electrons and protons. Prog. Photovolt. Res. Appl. *25*, 161–174.

Jena, A.K., Ikegami, M., and Miyasaka, T. (2017). Severe morphological deformation of Spiro-OMeTAD in $(CH_3NH_3)PbI_3$ solar cells at high temperature. ACS Energy Lett. *2*, 1760–1761.

Kogo, A., Ikegami, M., and Miyasaka, T. (2016). SnO_x-Brookite TiO_2 bilayer electron collector for hysteresis-less high efficiency plastic perovskite solar cells fabricated at low process temperature. Chem. Commun. *52*, 8119–8122.

Kojima, A., Teshima, K., Shirai, Y., and Miyasaka, T. (2009). Organometal halide perovskites as visible-light sensitizers for photovoltaic cells. J. Am. Chem. Soc. *131*, 6050–6051.

Lang, F., Nickel, N.H., Bundesmann, J., Seidel, S., Denker, A., Albrecht, S., Brus, V.V., Rappich, J., Rech, B., Landi, G., and Neitzert, H.C. (2016). Radiation hardness and self-healing of perovskite solar cells. Adv. Mater. *28*, 8726–8731.

Lee, M.M., Teuscher, J., Miyasaka, T., Murakami, T.N., and Snaith, H.J. (2012). Efficient hybrid solar cells based on meso-superstructured organometal halide perovskites. Science *338*, 643–647.

Li, Z., Zhu, Z., Chueh, C.-C., Luo, J., and Jen, A.K.-Y. (2016). Facile thiol-ene thermal crosslinking reaction facilitated hole-transporting layer for highly efficient and stable perovskite solar cells. Adv. Energy Mater. https://doi.org/10.1002/aenm.201601165.

Miyasaka, T. (2015). Perovskite photovoltaics: rare functions of organo lead halide in solar cells and optoelectronic devices. Chem. Lett. *44*, 720–729.

Mitzi, D.B. (1999). Synthesis, structure, and properties of organic–inorganic perovskites and related materials. Prog. Inorg. Chem. *48*, 1–121.

Morita, Y., Ohshima, T., Nashiyama, I., Yamamoto, Y., Kawasaki, O., and Matsuda, S. (1997). Anomalous degradation in silicon solar cells subjected to high-fluence proton and electron irradiations. J. Appl. Phys. *81*, 6491–6493.

Park, N.G., Grätzel, M., Miyasaka, T., Zhu, K., and Emery, K. (2016). Towards stable and commercially available perovskite solar cells. Nat. Energy *1*, 16152.

Saliba, M., Matsui, T., Seo, J.Y., Domanski, K., Baena, J.P.C., Nazeeruddin, M.K., Zakeeruddin, S.M., Tress, W., Abate, A., Hagfeldt, A., and Grätzel, M. (2016a). Cesium-containing triple cation perovskite solar cells: improved stability, reproducibility and high efficiency. Energy Environ. Sci. *9*, 1989–1997.

Saliba, M., Matsui, T., Domanski, K., Seo, J.Y., Ummadisingu, A., Zakeeruddin, S.M., Correa-Baena, J.P., Tress, W.R., Abate, A., Hagfeldt, A., and Grätzel, M. (2016b). Incorporation of rubidium cations into perovskite solar cells improves photovoltaic performance. Science *354*, 206–209.

Sanchez, R.S., and Mas-Marza, E. (2016). Light-induced effects on Spiro-OMeTAD films and hybrid lead halide perovskite solar cells. Sol. Energy Mater. Sol. Cells *158*, 189–194.

Singh, T., and Miyasaka, T. (2017). Stabilizing the efficiency beyond 20% with a mixed cation perovskite solar cell fabricated in ambient air under controlled humidity. Adv. Energy Mater. 1700677, https://doi.org/10.1002/aenm.201700677.

Smecca, E., Numata, Y., Deretzis, I., Pellegrino, G., Boninelli, S., Miyasaka, T., Magna, A.L., and Alberti, A. (2016). Stability of solution-processed

$MAPbI_3$ and $FAPbI_3$ layers. Phys. Chem. Chem. Phys. *18*, 13413–13422.

Stranks, S.D., Eperon, G.E., Grancini, G., Menelaou, C., Alcocer, M.J.P., Leijtens, T., Herz, L.M., Petrozza, A., and Snaith, H.J. (2013). Electron-hole diffusion lengths exceeding 1 micrometer in an organometal trihalide perovskite absorber. Science *342*, 341–344.

Sumita, T., Imaizumi, M., Matsuda, S., Ohshima, T., Ohi, A., and Itoh, H. (2003). Proton radiation analysis of multi-junction space solar cells. Nucl. Instrum. Methods Phys. Res. B *206*, 448–451.

Yamaguchi, M., Stephen, J.T., Matsuda, S., and Kawasaki, O. (1996). Mechanism for the anomalous degradation of Si solar cells induced by high fluence 1MeV electron irradiation. Appl. Phys. Lett. *68*, 3141.

Yang, W.S., Park, B.-W., Jung, E.H., Jeon, N.J., Kim, Y.C., Lee, D.U., Shin, S.S., Seo, J., Kim, E.K., Noh, J.H., and Seok, S.I. (2017). Iodide management in formamidinium-lead-halide–based perovskite layers for efficient solar cells. Science *356*, 1376–1379.

ISCI, Volume *2*

Supplemental Information

Tolerance of Perovskite Solar Cell to High-Energy Particle Irradiations in Space Environment

Yu Miyazawa, Masashi Ikegami, Hsin-Wei Chen, Takeshi Ohshima, Mitsuru Imaizumi, Kazuyuki Hirose, and Tsutomu Miyasaka

Transparent Methods

Device fabrication

Perovskite solar cells of different lead halide perovskite compositions were fabricated by solution-coating processes under ambient low humidity air according to the methods reported previously (Lee et al., 2012; Singh and Miyasaka, 2017) They were all mesoporous TiO_2-based structures built on F-doped tin oxide (FTO)-coated glass substrate. Indium tin oxide (ITO)-coated quartz substrate was specifically employed for tolerance examination against high energy electron beam, which was found to damage soda glass substrate. A TiO_2 compact layer (CL) for hole blocking function was prepared on the above conductive electrode substrates by spin coating 0.15 M precursor solution in 2-propanol of titanium diisopropoxide bis(acetylacetonate) at 6000 rpm for 30 s, which was heated at 125 ^{o}C for 5 min. Following this, same coating of CL was repeated twice with 0.3 M precursor solution and resultant film was sintered on a hotplate at 550 ˚C for 15 min, followed by UV ozone treatment (10 min) of the surface, to give a dense TiO_2 CL (thickness, ~50 nm). A mesoporous TiO_2 layer was prepared on the CL by a spin-coating of nano-TiO_2 particle dispersion (Solaronix, T/SP, diluted with ethanol in 2:7 weight ratio) at 6000 rpm for 30 s and sintered at 550^{o}C in air to form a mesoporous TiO_2 layer (thickness, ~200±50 nm). The TiO_2 layer was further treated with 0.02 M aqueous $TiCl_4$ (Aldrich) solution at 70^{o}C for 60 min and at 550^{o}C for 30 min. Various kinds of lead iodide perovskite materials were subjected to space environment examinations, which included mixed cation/halide perovskites such as Cl-doped $MAPbI_3$, Cs/$FAPbI_3$, FA/MAPb(I/Br)$_3$, and Cs/FA/MAPb(I/Br)$_3$, where MA and FA are methylammonium and formamidinium cations, respectively. Among them, we focused on two kinds of perovskite materials as summarized in this report, which were $Cs_xFA_{0.85}MA_{0.15}Pb(I_{0.85}Br_{0.15})_3$ (x<0.05) and Cl-doped $MAPbI_{3-x}Cl_x$, abbreviated as FAMAPb(IBr)$_3$ and $MAPbI_3$, respectively. Perovskite was crystalized on the above meso-TiO_2 scaffold layer by one step process. A 40 wt% solution containing 3M CH_3NH_3I and 1M $PbCl_2$ in N-dimethylformamide (DMF) was spin-coated on the scaffold layer at 2000 rpm for 30 s and was annealed at 110 ˚C for 90 min to form a $MAPbI_3$ layer. FAMAPb(IBr)$_3$ was prepared either by two step or one step solution process using DMF solutions of MA, FA, and Cs. The film was annealed at 155 °C for 90 min. For HTM, spiro-MeOTAD containing LiTFSI and TBP was used as a reference HTM material. It was coated on the perovskite layer from chlorobenzene solution and treated for oxidative doping under dry air for overnight. As a thermally stable HTMs, polymer hole conductor, P3HT, was spin-coated from a dichlorobenzene solution containing 15 mg ml^{-1} of P3HT, 15 uL of LiTFSI solution (170 mg mL^{-1} LiTFSI in acetonitrile) and 8 μL tert-butylpyridine (TBP) at 4000 rpm for 30 s. The dry HTM layer was annealed under ambient air at 50 ˚C for 5 min, followed by an additional annealing at 120 ˚C for 30 min. Finally, gold counter electrode was deposited by vacuum thermal evaporation. The cell substrate size was 1.25 × 1.25 cm on which 5 × 5mm square shaped solar cell was fabricated.

Photovoltaic performance measurements

On measurement photovoltaic characteristics, a black mask was mounted to confine the exposure area to be 3 × 3 mm. Photocurrent density–voltage (J–V) characteristics of the cell were measured under irradiation of 100 mW cm^{-2} (AM 1.5G, 1 sun) light supplied by a Peccell PEC-L11 solar simulator in combination with a Keithley 2400 source meter. In electron beam (EB) irradiation experiments, J–V curves before and after irradiation were measured under 136.7 mW cm^{-2} (AM 0G, 1 sun) light with an AM0 solar simulator (WXS-130S-L2HV AM0,WACOM) and a source meter (Agilent B2901A) at JAXA Tsukuba Space Center. External quantum conversion efficiency (EQE) was measured with a Peccell PEC-S20 action spectrum measurement system. Absolute incident power density of monochromatic light in EQE measurement was monitored based on a standard Si photodetector and was around 1 mW cm^{-2} at 550 nm. EQE measurement for the cells subjected to electron beam irradiation was specifically conducted at JAXA.

Space tolerance examinations

Thermal stability was examined by cyclic exposure of the encapsulated device to high and low temperatures of +100 ^{o}C and －80 ^{o}C for duration of 100 min to 7200 min (120 h) in Japan Aerospace Exploration Agency (JAXA) Sagamihara Campus Laboratory by encapsulating cells with glass sheets and a hot-melt type gasket sealing film (Himilan 1652, DuPont-Mitsui Polychemicals). Electron radiation tolerance was measured by using ITO/quartz substrate-based devices under vacuum and irradiation of 1 MeV electron beam supplied by a Cockcroft Walton accelerator in Takasaki Advanced Radiation Research Institute (TARRI), National Institutes for Quantum and Radiological Science and Technology (QST), Japan. Proton radiation tolerance was measured under irradiation of 50 KeV proton beam supplied by an ion implanter at Wakasa Wan Energy Research Center, Japan.

Supplemental Data

Photovoltaic characteristics of P3HT-based perovskite cells

Perovskite solar cells with different perovskite compositions employed in electron and proton irradiation tolerance experiments had photocurrent—voltage characteristics as shown in Figure S1. Their photovoltaic performance parameters are summarized in Table S1.

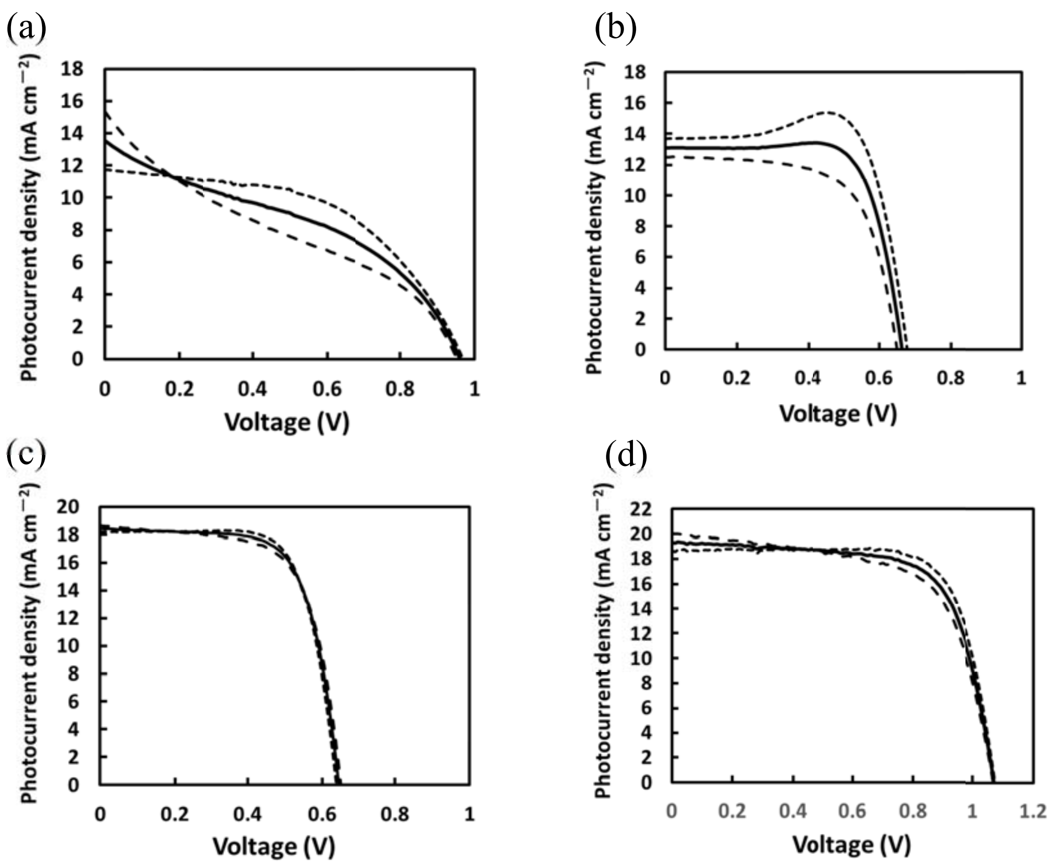

Figure S1. J–V characteristics of P3HT-based perovskite solar cells employed for electron and proton irradiation tolerance examinations: (a) FAMAPb(IBr)$_3$ and (b) $MAPbI_3$ cells. (c) $MAPbI_3$ cell of highest efficiency (8.2%), (d) J–V characteristics of spiro-OMeTAD-based perovskite cell employed as a reference sample.

——— average, – – – forward scan, ·········· backward scan. Bias voltage scanning was carried out at step voltage of 0.01 V, delay time of 0.05 s, and scanning rate of 140 mV s^{-1}. Related to Figure 1 showing the device structures (SEM cross sections) of P3HT-based FAMAPb(IBr)$_3$ and $MAPbI_3$ perovskite solar cells.

Table S1. J-V characteristics of perovskite solar cells (TiO_2/perovskite/P3HT/Au) employed in radiation tolerance examination. J_{SC}, V_{OC}, FF, and PCE, measured under 100 mW cm^{-2} simulated sunlight, are average values of forward and back scans of J-V curves which exhibited a relatively large hysteresis (Figure S1). Range of values indicates variation coefficient for 15 cells. Related to Figure 1.

Perovskite composition	J_{SC} (mA/cm^2)	V_{OC} (V)	FF	PCE (%)
$MAPbI_3$	12.5±0.4	0.66±0.01	0.57±0.03	4.8±0.3
$FAMAPb(IBr)_3$	13.6±0.5	0.94±0.00	0.35±0.01	4.4±0.1

Thermal stability examinations

The results of thermal stability at high (100°C) and low (−80°C) temperatures for perovskite solar cells with different perovskite compositions are summarized in Table S2. A cell using spiro-OMeTAD as reference is also compared, which showed poor stability at high temperature and was not subjected to radiation tolerance measurements. Figure S2 shows changes of photovoltaic parameters (J_{SC} and V_{OC}) of P3HT-based $FAMAPb(IBr)_3$ and $MAPbI_3$ encapsulated cells by 120 h exposure to high and low temperatures.

Table S2. Impact of high and low temperatures in terms of remaining factor (%) of J_{SC} and V_{OC} values for P3HT-based $MAPbI_3$ and $FAMAPb(IBr)_3$ perovskite cells (encapsulated) under continuous 1000min (16.7 h) and 7200 min (120 h) exposure to 100 °C and −80 °C air-free atmosphere. spiro-OMeTAD based cell (as a reference) mostly lost its photovoltaic activity in 1000 min. Related to Figure 1, 2, 4, and 5. Based on these stability results, P3HT-based perovskite cells were chosen for electron and proton irradiation tests as shown in Figure 2, 4, and 5.

Perovskite (HTM)	$MAPbI_3$ (spiro-OMeTAD)	$MAPbI_3$ (P3HT)		$FAMAPb(IBr)_3$ (P3HT)
Duration	1000 min (16.7 h)	1000 min (16.7 h)	7200 min (120 h)	7200 min (120 h)
+100°C	PCE dropped to <20 % (J_{SC} remained <40% in first 100 min)	J_{SC} 157 ± 28% V_{OC} 91 ±1%	J_{SC} 57 ± 31% V_{OC} 123 ±11%	J_{SC} 93 ± 10% V_{OC} 97 ±12%
−80°C	—	J_{SC} 99 ± 23% V_{OC} 101 ±2%	J_{SC} 101 ± 14% V_{OC} 117 ±11%	J_{SC} 82 ± 30% V_{OC} 104 ±6%

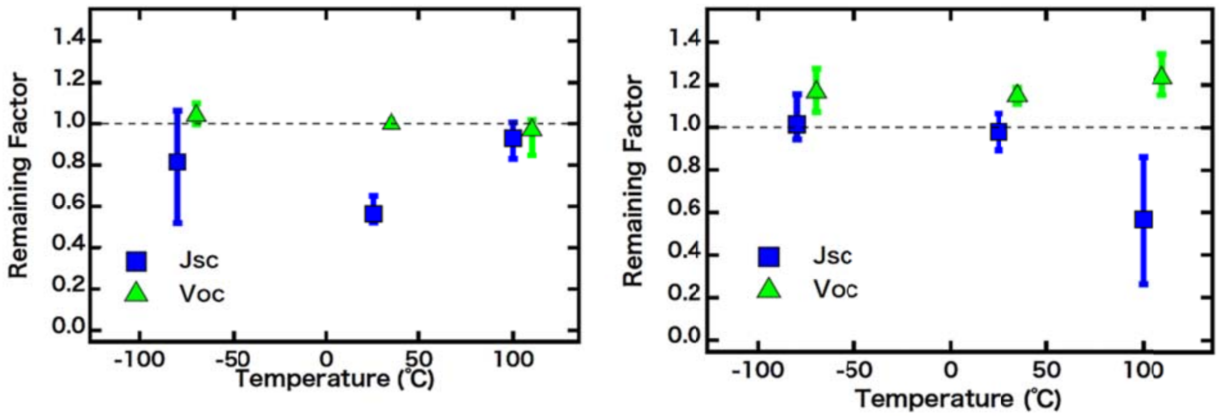

Figure S2. Influences of temperature changes on photovoltaic parameters (J_{SC} and V_{OC}) of P3HT-based FAMAPb(IBr)$_3$ (left) and MAPbI$_3$ (right) encapsulated perovskite cells for prolonged 120 h exposure to 100 ^oC, room temperature, and −80 ^oC. Situations of J_{SC} and V_{OC} points are laterally separated to avoid overlapping. Error bar represents distribution of values from 5 cells. Related to Figure 1.

Figure S3 shows photographs of perovskite sample cells employed for proton irradiation test, comparing the color of perovskite layer before and after irradiation of high fluence 50 KeV proton beam.

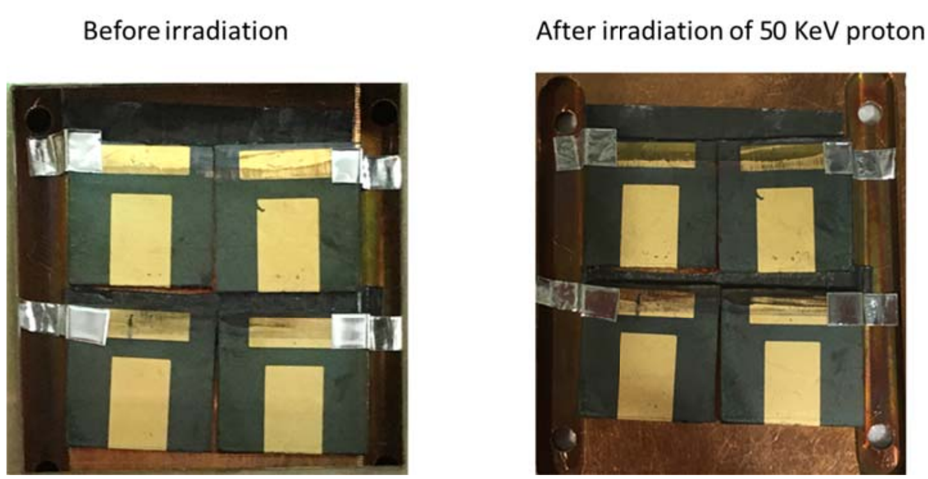

Figure S3. Perovskite cell samples before and after the irradiation of 50 KeV proton with fluence of 10^{14} particles cm^{-2}, showing no change in color (no sign of yellow PbI$_2$ precipitation) occurring on perovskite layers. Black areas surrounding gold electrodes show perovskite layers. Related to Figure 4 (proton-induced changes in EQE spectra) and Figure 5 (changes in J-V curve parameters).